PHYSICAL REVIEW C

NUCLEAR PHYSICS

THIRD SERIES, VOL. 5, NO. 6 June 1972

Elastic Scattering of Lithium by Carbon*

J. E. Poling, E. Norbeck, and R. R. Carlson

Department of Physics and Astronomy, The University of Iowa, Iowa City, Iowa 52240

(Received 8 December 1971)

The elastic scattering cross sections of Li^6 and Li^7 on C^{12} were measured at a number of bombarding energies from 4.5 to 13 MeV. The ratio of the cross section to the Rutherford cross section was determined for a wide range of angles at each energy. The data were fitted by an optical-model potential with four parameters: radius, diffuseness, real well depth, and imaginary surface-absorption well depth. All data for each isotope could be fitted with numerous sets of parameters with real well depths between 40 and 450 MeV. Data for both isotopes could be fitted using the same values for radius and diffuseness and essentially the same for real well depth, but with greater imaginary well depth for Li^7. The fit holds good for all energies if a linear dependence of the imaginary well depth on energy is included. Data are also expressed in terms of the nuclear parts of the collision matrix elements which show certain regularities. As a by-product of this work, it was found that in the elastic scattering of lithium by gold the screening of the gold nucleus by its inner electrons is important for energies below 3.0 MeV.

I. INTRODUCTION

Elastic scattering of beams of simple nuclei has long been used to obtain information about nuclear structure and reaction mechanisms. Results have commonly been fitted using an optical-model potential. This procedure has recently been extended to the results of elastic scattering studies made with beams of more complex nuclei. The potentials obtained for such cases are difficult to interpret physically, and one might question whether any physical meaning at all could be attributed to a potential representing the interaction of two complex nuclei. The present work was undertaken to see whether the elastic scattering of the lightest nuclei in the $1p$ shell (the lithium isotopes) could be represented by a potential function over an extended energy range. The target material was carbon.

Elastic scattering of Li^6 by C^{12} has been studied at 20 MeV at Heidelberg[1] and 13 MeV at Iowa.[2] Optical-model fits were made to the data with reasonable success. The scattering of Li^7 by C^{12} has been studied at 7.3 MeV.[3] Optical-model fits were again reasonably successful. In the present work the scattering has been measured at a number of bombarding energies from 4.5 to 13 MeV. This energy range spans the Coulomb barrier. The combined requirements of fitting data from a broad energy range and two isotopes should limit the parameters of the optical-model potential.

II. METHOD

Elastic scattering measurements were made with lithium beams supplied by the University of Iowa Van de Graaff accelerator. Either Li^6 or Li^7 beams could be selected from a multiple hot-filament ion source. Positively charged ions in either the single-, double-, or triple-charge state were accelerated to energies up to 13 MeV. The beam was collimated and brought to the cen-

ter of a 17-in.-diam ORTEC Model No. 600 scattering chamber. Targets were self-supporting carbon foils from 5 to 50 $\mu g/cm^2$ thick. A thin layer of gold was placed on most of the targets for use in monitoring the beam. The differential cross section for elastic scattering was measured with these beams and targets for angles from as far forward as 6.0° to as far back as 120° in the laboratory, and for bombarding energies of 4.5, 5.8, 6.4, 7.5, 9.0, 11.0, and 13.0 MeV. Not all of these energies were used in the case of Li^7.

At beam energies of 7.5 MeV and above, an *E-dE* detector system was used to identify the elastically scattered lithium nuclei. These have to be separated from inelastically scattered particles and reaction products, mostly α particles. At the lower bombarding energies the only inelastic scattering is that of the Li^7 beam particle itself, but at higher energies the first excited state of carbon is excited for both beams. The *dE* detector was 7.5-μ-thick silicon; the *E* detector was 150-μ-thick silicon. The detector telescope subtended an angle of 1.0° at the target. Most proton and deuteron reaction products left little energy in these detectors and, therefore, were not confused with the elastic lithium particles. This system was not used for energies below 7.5 MeV because the elastically scattered lithium could not penetrate the *dE* detector for backward angles. At 7.5 MeV, data could be taken as far back as 80° in the laboratory.

Pulses from the two detectors were digitized and then taken in by an on-line computer (CDC 160-A). Data were stored in a two-dimensional array with 60×256 positions for *dE* versus *E*. Particle identification was made after the run on the basis of known energy-loss curves for the different particles. A pulse-height distribution for lithium products was plotted and the various peaks identified on the basis of their energy. The elastic scattering yield was taken as the sum under the proper peak. This peak was usually the largest one in the spectrum.

At beam energies of 6.4 MeV and below, a single 150-μ-thick silicon detector was used. It subtended an angle of 1.0°. Reaction peaks and elastic peaks were separated on the basis of energy. When elastic and reaction peaks coincided, the size of the reaction peak was estimated from its size at other angles where it was separated. This method was limited to angles forward of 115° in the laboratory because of the decreasing size of the elastic peak in relation to the reaction peaks as the scattering angle increased.

A position-sensitive detector[4] was used in place of the single detector to look for small oscillations in the elastic yield at forward angles. Such oscillations were predicted on the basis of optical-model fits. Careful measurements were made with a Li^6 beam at 5.8 MeV at laboratory angles greater than 6°. The detector was 9° across. It gave two signals, with one proportional to energy deposit and the other proportional to position times energy. These signals were digitized by two analog-to-digital-converter units and then stored by the on-line computer for later analysis on an IBM 360/65 computer. The detector was carefully calibrated across its face for efficiency and angle using an α-particle source. After the run, the data were separated into groups from

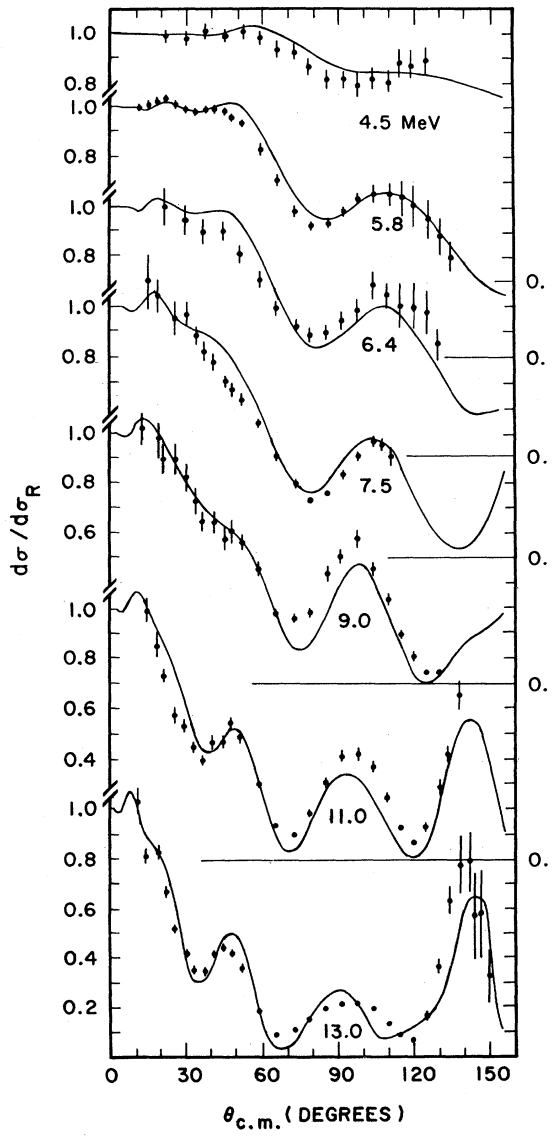

FIG. 1. Ratio of the elastic scattering cross section to the Rutherford cross section for Li^6 on C^{12}. Numbers under the curves are laboratory bombarding energies. Curves were calculated using parameter Set B.

nine, 1°-wide, contiguous regions. For the forward angles the detector was moved in 2° steps to get overlap, and the measured region was covered several times. At backward angles the overlap and number of runs were reduced. The data are given here for a sufficient number of angles to show the oscillations clearly.

Oxygen and other contaminants in the target produced elastic peaks which merged with the elastic peak due to carbon at laboratory angles forward of 20°. The contribution from these contaminants was subtracted on the basis of the behavior of the contaminant elastic peak before it merged with the carbon elastic peak. The amounts subtracted were usually less than 5% of the elastic peak. In some cases, such as the experiment done with the position-sensitive detector, thin targets of 5 to 10 $\mu g/cm^2$ were used for better resolution at the forward angles. The percentage content of oxygen was somewhat higher in these cases.

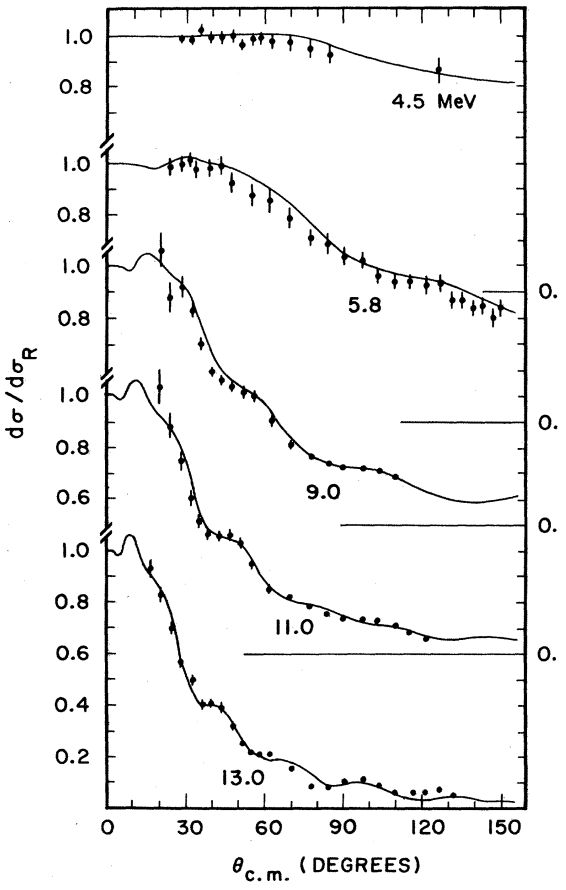

FIG. 2. Ratio of the elastic scattering cross section to the Rutherford cross section for Li^7 on C^{12}. Numbers under the curves are laboratory bombarding energies. Curves were calculated using parameter Set B.

Throughout the present energy range the scattering off gold was expected to be pure Rutherford scattering. Beam current for runs at different angles was monitored on this basis. The thin gold layer on the front face of the target provided an elastic peak which was well separated from other peaks in the spectrum.

To put the angular distributions on an absolute basis, it was necessary to know the relative number of carbon and gold atoms. This was found by measuring the ratio of the carbon and gold elastic scattering peaks as a function of bombarding energy. These yield curve measurements were made at 40° from 13 MeV down to 3.0 MeV bombarding energy. The ratio remained constant below 4.0 MeV, indicating that the scattering off carbon was Rutherford at these energies. Consequently, angular distributions were reduced to the ratio of measured cross section to Rutherford cross section by comparison with the yield curves at 40°. Energy losses in the gold were negligible, but the carbon was thick enough to require corrections of up to 50 keV to give the true bombarding energy at the target center. Some thickening of the targets due to carbon buildup was observed, and corrections were applied where appropriate.

Normalization was done at 3.0 MeV and not lower, because at lower energies the screening of the gold nucleus by its inner electrons became important. This was demonstrated both by classical orbit calculations and by laboratory measurements for lithium beam energies of 3.0, 2.0, 1.5, and 0.65 MeV. For a 60° angle the cross section was smaller than the Rutherford scattering cross section by 2% at 3.0 MeV and by 13% at 0.65 MeV.

Additional beam-current monitoring for individual angular distributions at beam energies of 7.5 MeV and above was provided by a stationary detector. This detector was covered by a nickel foil to screen out elastically scattered particles so that it would monitor only reaction products.

In Figs. 1 and 2 the ratio of measured cross section to Rutherford cross section is plotted as a function of center-of-mass angle for lithium. The curves through the points are optical-model fits

TABLE I. Optical-model parameter sets.

			Li^6+C^{12}			Li^7+C^{12}		
	R (F)	a (F)	V (MeV)	$W_{4.5}$ (MeV)	W_{13} (MeV)	V (MeV)	$W_{4.5}$ (MeV)	W_{13} (MeV)
A	3.50	0.65	138	6.5	8.8	157	12.0	25.0
B	3.37	0.65	148	6.9	8.5	166	12.0	26.0
C	3.21	0.63	209	7.9	10.2	232	9.0	32.0
D	3.21	0.59	332	7.8	14.5	350	18.0	35.0
E	3.21	0.58	403	13.0	18.0	420	19.0	40.0

and are discussed below. The laboratory bombarding energy is indicated below each set of data. It should be noted that the data are shown in linear plots.

Various sources of error contribute to the errors indicated on the points in the figures. At forward angles the subtraction of scattering from oxygen and heavier materials is the major contributor. At backward angles statistics are a major contributor. For lower bombarding energies an occasional α-particle group interferes with the elastic scattering for a few angles. Energy loss in the carbon target has to be introduced as a correction and this causes possible error in the calculated Rutherford cross section. Finally, the data depend on the accuracy of the yield curve for absolute value. All of these sources are combined into a standard deviation error for each point in the figures. In case no error bars are shown, the error is smaller in size than the point.

III. OPTICAL-MODEL CALCULATIONS

The data shown in Figs. 1 and 2 were fitted by numerically integrating the Schrödinger equation for the lithium-carbon scattering process to get the real and imaginary parts of the collision matrix for the first fifteen partial waves and from these, the cross section.[5] The higher partial waves had little effect on the cross section. Only the first 5 were important at 5.8 MeV, and only the first 10 at 13 MeV. The numerical integration was carried out to 15 F, though 10 F was sufficient. For the results presented here, the integration step size was 0.05 F; calculations were done in double precision on an IBM 360/65 computer. Calculations were checked for stability as the step size was varied from 0.025 to 0.25 F. Results remained essentially unchanged for step sizes below 0.15 F. For selected cases, the results of the program were compared with those from two other programs that used different numerical-integration techniques.[6,7] The agreement was good.

The optical-model potential had the following form:

$$V(r) = -Vf(r) - iW\left(-4a\frac{df}{dr}\right) + V_C(r),$$

$$f(r) = (1 + e^{(r-R)/a})^{-1}.$$

The Coulomb potential, V_C, was that due to a uniform distribution of charge extending out to the nuclear radius R. Searches were conducted on all four parameters, V, R, a, and W, to get good fits to the data.[5] Searching on all parameters at once generally did not give good results. The best results came from optimizing two parameters at a time. After several good fits were obtained, the pattern of values of R and V giving such fits would begin to emerge and could be used as a guide. Table I lists a number of acceptable

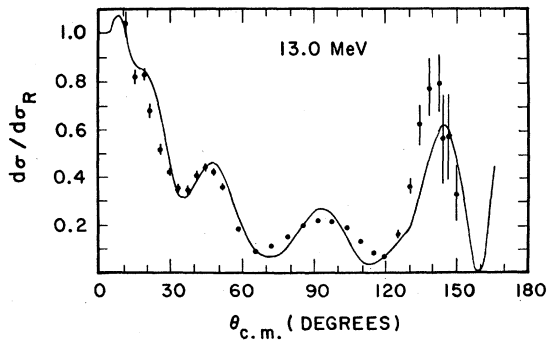

FIG. 3. Ratio of the elastic scattering cross section to the Rutherford cross section for 13-MeV Li^6 on C^{12}. The curve was calculated using parameter Set E.

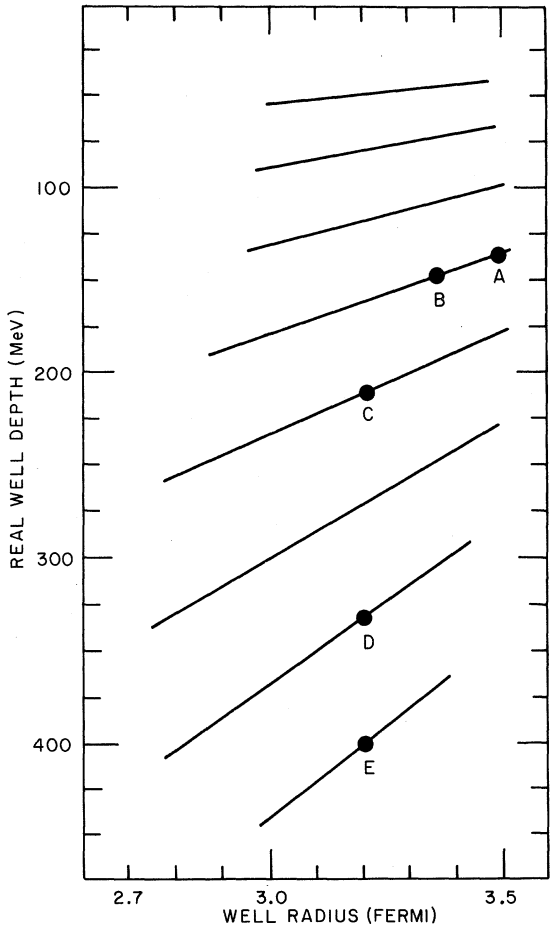

FIG. 4. Lines indicate loci of R, V values giving a good fit to the 13-MeV data for elastic scattering of Li^6 by C^{12}. Letters denote parameter sets of Table I.

parameter sets. These sets give good fits to both reactions over the whole energy range. The imaginary well depth W varies linearly with energy between the extremes given in Table I: $W_{4.5}$, depth at 4.5 MeV; and W_{13}, depth at 13.0 MeV. Set B was used to calculate the curves drawn in Figs. 1 and 2. Figure 3 shows a fit calculated using Set E, where the well depth is markedly greater than it is in Set B.

Parameter sets which give adequate fits to the data fall into families. Figure 4 shows lines giving values of R versus V for good fits to Li^6+C^{12} at 13-MeV bombarding energy. A line marks a locus of good fits. Each locus corresponds to a different number of half wavelengths inside the well. Points corresponding to the various parameter sets in Table I are marked on the lines in Fig. 4. In order to get a good fit along the length of the lines shown, small variations in a and W were necessary.

Considerable effort was spent trying to find fits with reasonable radii and small V, corresponding to the region in Fig. 4 above the top line. For well depths near 30 MeV, the peaks were in the right place, but had incorrect relative heights. Good fits were not possible.

The fits reported here used a surface-absorption form for the imaginary well. Volume-absorption wells were also investigated and gave almost identical results. A spin-orbit potential term was tried but was not found to be useful.

Extensive fitting was also done with a six-parameter potential in which the imaginary well radius and diffuseness were allowed to become different from the real well radius and diffuseness. In most cases the radius and diffuseness of the real well remained essentially the same as in the four-parameter fits, but the radius and diffuseness of the imaginary well always increased. Slightly better fits to individual angular distributions were possible with six parameters, which is to be expected when two more parameters are made available. However, the six-parameter fits for either Li isotope over the entire range were of the same quality as the four-parameter fits.

The parameter sets which give the best fits to the data at each bombarding energy all result in essentially the same values of the collision matrix U_l. Therefore, the collision matrix elements give a useful representation of the data. Thus:

$$\frac{d\sigma}{d\Omega}=\left|f_C(\theta)+\frac{1}{2ik}\sum_{l=0}^{15}(2l+1)(e^{2i\omega_l}-U_l)P_l(\cos\theta)\right|^2.$$

The quantity, $f_C(\theta)$, is the Coulomb amplitude.[8] If there were no nuclear potential, U_l would equal

TABLE II. Partial-wave amplitudes for Li^6+C^{12}.

l	4.5 (MeV)	5.8 (MeV)	6.4 (MeV)	7.5 (MeV)	9.0 (MeV)	11.0 (MeV)	13.0 (MeV)
0	0.714	0.413	0.368	0.334	0.316	0.299	0.283
	360°	321°	297°	254°	203°	141°	86°
1	0.923	0.686	0.564	0.396	0.282	0.237	0.227
	3°	6°	5°	359°	346°	320°	286°
2	0.915	0.585	0.468	0.371	0.330	0.305	0.284
	3°	356°	342°	310°	267°	221°	179°
3	0.990	0.921	0.850	0.665	0.419	0.243	0.195
	1°	355°	8°	14°	18°	22°	21°
4	0.996	0.961	0.903	0.713	0.482	0.366	0.318
	0°	3°	5°	6°	351°	320°	293°
5	1.000	0.996	0.990	0.964	0.864	0.586	0.307
	0°	1°	1°	4°	11°	24°	37°
6	1.000	1.000	0.998	0.990	0.949	0.774	0.565
	0°	0°	0°	1°	4°	9°	6°
7	1.000	1.000	1.000	0.998	0.994	0.967	0.881
	0°	0°	0°	0°	1°	5°	12°
8	1.000	1.000	1.000	1.000	0.998	0.992	0.969
	0°	0°	0°	0°	0°	2°	4°
9	1.000	1.000	1.000	1.000	1.000	0.998	0.994
	0°	0°	0°	0°	0°	0°	1°

TABLE III. Partial-wave amplitudes for Li^7+C^{12}.

l	4.5 (MeV)	5.8 (MeV)	9.0 (MeV)	11.0 (MeV)	13.0 (MeV)
0	0.853	0.486	0.133	0.083	0.058
	3°	352°	246°	172°	104°
1	0.914	0.647	0.202	0.110	0.064
	1°	356°	286°	226°	166°
2	0.957	0.720	0.206	0.120	0.080
	2°	4°	306°	249°	193°
3	0.986	0.893	0.361	0.194	0.110
	1°	3°	344°	308°	265°
4	0.998	0.967	0.514	0.283	0.171
	0°	2°	2°	338°	304°
5	1.000	0.994	0.783	0.499	0.294
	0°	1°	7°	3°	347°
6	1.000	0.998	0.932	0.746	0.502
	0°	0°	4°	8°	5°
7	1.000	1.000	0.984	0.923	0.767
	0°	0°	1°	5°	9°
8	1.000	1.000	0.996	0.978	0.923
	0°	0°	0°	2°	4°
9	1.000	1.000	0.998	0.994	0.978
	0°	0°	0°	1°	2°

$e^{2i\omega_l}$. Consequently, to show the effects of the nuclear potential, Table II lists the values of the partial-wave amplitudes, $\eta_l = e^{-2i\omega_l} U_l$, for the reaction $Li^6 + C^{12}$. These values correspond to the fits shown in Fig. 1. Table III does the same for $Li^7 + C^{12}$.

Figure 5 shows partial-wave amplitudes for the two reactions plotted on Argand diagrams. Lines are drawn connecting matrix elements corresponding to a particular l value. Bombarding energy is denoted by point shape. The $Li^7 + C^{12}$ values generally follow a common track so only the $l = 0$ amplitude is shown. The phase angle first increases and then decreases, and the magnitude shrinks as the energy increases. The $Li^6 + C^{12}$ values do the same except that the magnitude is larger, and the even and odd angular momentum amplitudes follow quite different tracks.

IV. CONCLUSION

The optical model does provide a successful description for elastic scattering of lithium from carbon. Both Li^6 and Li^7 scattering from C^{12} can be fitted over a wide energy range with wells of the same radius and diffuseness, and only slightly different depths. The parameter sets listed in Table I are a few of the many sets which give good fits to the data. The analysis showed that the real well depth must not be less than about 40 MeV. Except for this limitation, loci of good fits were found throughout the physically meaningful regions for the radius and real-well-depth parameters. We assumed that the real well could not be much deeper than the sum of the real well depths for all of the nucleons in the lithium nucleus scattering individually, so we did not search at well depths greater than about 450 MeV.

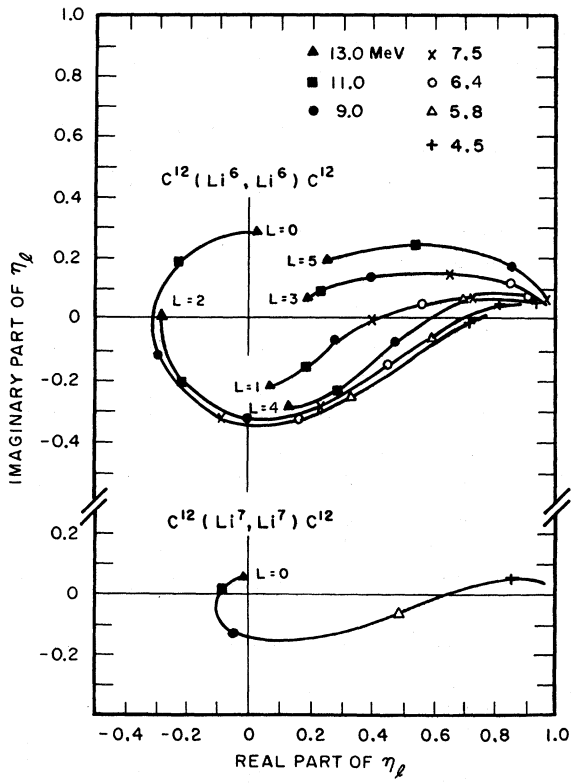

FIG. 5. Real vs imaginary parts of η_l for Li^6 on C^{12} and Li^7 on C^{12}. Points are plotted for each bombarding energy as indicated, and lines connect points with common l value.

A large number of possible values for the real well depth V is the usual result of trying to fit elastic scattering cross sections for composite particles. Techniques have been developed for estimating the physically meaningful potential. The method of Kadmenskii[9] calculates the potential by averaging the radial functions of the optical potentials for the constituent nucleons over the spatial density of these nucleons in the composite particle. For the scattering of Li^6 from C^{12}, this method gives numbers such as 200 MeV for V.[10] Roughly the same results are obtained when the calculation is done by Watanabe's method[11] using a d-α cluster structure instead of a density distribution.[12]

In the elastic scattering of composite particles one can question whether the core of the well is important, since only low l values are affected by the core, and absorption of these partial waves is likely. In order to test this idea, repulsive cores of several different shapes and of about 0.5-F radius were added to the Woods-Saxon well corresponding to parameter Set B. The partial-wave amplitudes were markedly changed for low

TABLE IV. Total reaction cross sections.

Energy (MeV)	Calculated values for $Li^6 + C^{12}$ (mb)	Measured values for $Li^6 + C^{12}$ (mb)	Calculated values for $Li^7 + C^{12}$ (mb)	Measured values for $Li^7 + C^{12}$ (mb)
4.5	110	36 [a]	75	6 [b]
5.8	320	90 [c]	290	12 [b]
6.4	410	105 [c]		
7.5	560			
9.0	690	124 [d]	730	70 [e]
11.0	810	107 [d]	880	75 [e]
13.0	880	91 [d]	970	47 [e]

[a] Reference 13. Sum of p_0-p_4, d_0-d_4, α_0-α_2.
[b] Preliminary results. Sum of p_0-p_4, d_0-d_1, t_0, α_0.
[c] Reference 2. Sum of p_0-p_3, d_0-d_4, α_0-α_2.
[d] Reference 2. Sum of p_0-p_4, d_0-d_5, α_0-α_4.
[e] Preliminary results. Sum of p_0-p_4, d_0-d_3, t_0-t_4, α_0-α_3.

l values. One concludes that in the case of lithium-carbon scattering, even the innermost parts of the potential well are important.

The total reaction cross section can be calculated from the partial-wave amplitudes given in Tables II and III for each bombarding energy and reaction. The results are shown in Table IV. The measured values are less than the total because of the unmeasured particle groups. There are also continua in the spectra of outgoing particles which have not been included in the sum.[2,13] From qualitative observation of these continua it is quite possible that they could account for the remaining cross section. The similarity in the calculated cross sections was unexpected in view of the difference in the pattern of the partial-wave amplitudes shown in Fig. 5.

The elastic scattering of Li^6 and Li^7 by carbon is different in character in the energy range covered in this work. The former shows diffractive behavior in its angular distributions, whereas the latter has almost smooth angular distributions. This difference is seen also in Fig. 5 in the way the partial-wave amplitudes depend on the energy. The Li^6 amplitudes are generally larger than the corresponding Li^7 amplitudes and show an alternation in the behavior of the even and odd partial waves. For Li^6 the phase of the odd partial waves does not change nearly as rapidly as that of the even waves. The physical reason for this is not understood.

ACKNOWLEDGMENT

We would like to acknowledge the assistance of Dr. D. J. Johnson in the early stages of this work, and of Professor G. L. Payne in the theoretical analysis.

---

*Work partially supported by the National Science Foundation.

[1]K. Bethge, K. Meier-Ewert, and K. O. Pfeiffer, Z. Physik 208, 486 (1968).

[2]D. J. Johnson and M. A. Waggoner, Phys. Rev. C 2, 41 (1970).

[3]J. R. J. Bennett and I. S. Grant, in *Proceedings of the Third Conference on Reactions Between Complex Nuclei*, edited by A. Ghiorso, R. M. Diamond, and H. E. Conzett (University of California Press, Berkeley, 1963), p. 50.

[4]E. Norbeck and R. R. Carlson, *Instrumentation Techniques in Nuclear Pulse Analysis* (National Academy of Sciences, National Research Council, Washington, D. C., 1964), Publication No. 1184, p. 42.

[5]W. R. Smith, University of Southern California Report No. 136-119, 1967 (unpublished).

[6]E. H. Auerbach, Brookhaven National Laboratory Report No. BNL-6562 (unpublished).

[7]G. L. Payne, private communication.

[8]A. M. Lane and R. G. Thomas, Rev. Mod. Phys. 30, 257 (1958).

[9]S. G. Kadmenskii, V. E. Kalechits, S. I. Lopatko, V. I. Furman, and V. A. Khlebostroev, Yadern. Fiz. 10, 730 (1969) [transl.: Soviet J. Nucl. Phys. 10, 422 (1970)].

[10]G. L. Payne, private communication.

[11]S. Watanabe, Nucl. Phys. 8, 484 (1958).

[12]J. W. Watson, Optical Potentials for the Elastic Scattering of ^{6}Li Ions, Texas A & M University (to be published); and private communication.

[13]D. W. Heikkinen, Phys. Rev. 141, 1007 (1966).